

# VID-LLM: A COMPACT VIDEO-BASED 3D MULTIMODAL LLM WITH RECONSTRUCTION-REASONING SYNERGY

Haijier Chen<sup>1\*</sup>, Bo Xu<sup>1\*</sup>, Shoujian Zhang<sup>1†</sup>, Haoze Liu<sup>1</sup>, Jiaxuan Lin<sup>1</sup>, Jingrong Wang<sup>2</sup>

<sup>1</sup> School of Geodesy and Geomatics, Wuhan University

<sup>2</sup> School of Architecture and Urban Planning, Shenzhen University

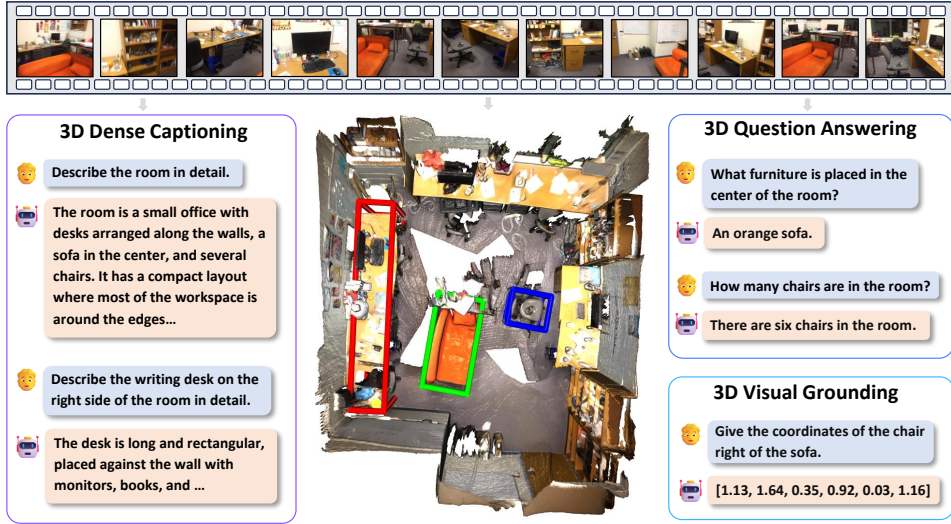


Figure 1: We propose **Vid-LLM** to achieve diverse 3D vision-language reasoning tasks using only video inputs.

## ABSTRACT

Recent developments in Multimodal Large Language Models (MLLMs) have significantly improved Vision-Language (VL) reasoning in 2D domains. However, extending these capabilities to 3D scene understanding remains a major challenge. Existing 3D Multimodal Large Language Models (3D-MLLMs) often depend on 3D data inputs, which limits scalability and generalization. To address this limitation, we propose Vid-LLM, a video-based 3D-MLLM that directly processes video inputs without requiring external 3D data, making it practical for real-world deployment. In our method, the geometric prior are directly used to improve the performance of the scene perception. To integrate the geometric cues into the MLLM compactly, we design a Cross-Task Adapter (CTA) module to align the 3D geometric priors with the vision-language representations. To ensure geometric consistency and integrity, we introduce a Metric Depth Model that recovers real-scale geometry from the reconstruction outputs. Finally, the model is fine-tuned with a two-stage distillation optimization strategy, realizing fast convergence and stabilizes training. Extensive experiments across diverse benchmarks verified the effectiveness of our method on 3D Question Answering, 3D Dense Captioning and 3D Visual Grounding tasks, demonstrating the superior multi-task capabilities. Code and data are available on <https://chenhaijier.github.io/Vid-LLM/>.

\* Equal contribution.

† Corresponding authors.

## 1 INTRODUCTION

Recent advances in Large Language Models (LLMs) (Vaswani et al., 2017; Radford et al., 2019; Naveed et al., 2025) and Multimodal Large Language Models (MLLMs) (Zhang et al., 2024a; Yin et al., 2024; Wu et al., 2023) have reinforced the paradigm of language as a universal interface, substantially improving cross-modal perception and reasoning. Extending this progress to 3D, recent research has focused on 3D-aware Multimodal Large Language Models (3D-MLLMs) (Ren et al., 2025), which unify 3D scene understanding and vision–language reasoning under a linguistic interface. This line of work underscores the importance of grounding language in persistent 3D spatial representations (Cheng et al., 2024a; Roh et al., 2022), offering a unified pathway toward systematic scene-level reasoning.

Recent studies have made substantial progress in 3D vision–language (3D VL) reasoning (Chen et al., 2024c; Huang et al., 2023b), yet most approaches rely on complex 3D inputs, incurring high costs in data collection, preprocessing, and computation. Some models rely on point clouds or reconstructed scenes augmented with rendered views or semantic–geometric features (Hong et al., 2023a; Fu et al., 2024), while others adopt simpler inputs but still depend on explicit 3D scene representations such as reconstructed objects aligned with semantic representations (Chu et al., 2024; Huang et al., 2023a; 2024). Despite their effectiveness, these pipelines depend on depth, poses, or external modules, leading to substantial data and engineering overhead as well as high memory and latency costs. This rigid input requirements and system complexity fundamentally limit the scalability and transferability of current 3D-MLLMs.

To overcome these limitations, a more general solution is to enable the model to directly reconstruct scene geometry from video (Leroy et al., 2024; Wang et al., 2024), thereby eliminating the reliance on external depth, pose, or registration modules. More importantly, reconstruction and reasoning are intrinsically interdependent: geometric structures underpin semantic understanding, while semantic reasoning, in turn, provides contextual priors that guide and refine geometric modeling (Cheng et al., 2024a; Ha & Song, 2022).

In this work, we introduce Vid-LLM, a compact model that jointly performs reconstruction and 3D vision–language reasoning from monocular video inputs, as illustrated in Fig. 1. The core component of Vid-LLM is a Cross-Task adapter (CTA) that tightly couples reconstruction with reasoning, enabling intrinsic geometry–semantics interaction with mutual reinforcement and constraint. CTA disentangles geometry-aware and language-aware features; the geometric stream is then processed by a Global-Frame Attention backbone and specialized heads to estimate camera poses and relative depth, followed by a Metric Depth Model for real-scale calibration. The recovered 3D information is then fused with semantic features to construct 3D patches, which are fed into the LLM for spatial reasoning. Finally, a two-stage training strategy ensures convergence and improves overall performance. Extensive experiments across diverse 3D vision–language benchmarks demonstrate the performance of Vid-LLM and confirm its effectiveness as a practical and scalable framework for video-based 3D multimodal reasoning.

Our main contributions are summarized as follows:

- We propose Vid-LLM for versatile 3D scene understanding. The framework does not rely on dense 3D inputs or prior poses, making it practical for real-world deployment.
- We design a Cross-Task adapter to align the 3D geometry priors with VL representations, boosting the integration of 3D visual geometry priors into MLLM. A two-stage training strategy is further adopted to improve the stability and performance.
- Extensive experimental evaluations are conducted on real datasets to evaluate the performance of our method. The experimental results demonstrate that our method achieves superior performance in terms of question answering, dense captioning and visual grounding. We will publish our code to facilitate communication.

## 2 RELATED WORK

3D-MLLMs have achieved significant advances in 3D scene understanding, yet their reliance on explicit 3D data still limits scalability and applicability. Meanwhile, progress in 3D reconstruction

shows that geometry can be directly reconstructed from videos. Integrating such geometric priors into 3D-MLLMs represents a promising approach to enhance semantic grounding. We therefore review related work in three directions: (i) 3D-MLLMs, (ii) 3D reconstruction, and (iii) geometry priors in vision-language models.

**3D-aware Multimodal Large Language Models (3D-MLLMs).** 3D-MLLMs aim to unify 3D scene understanding and vision–language reasoning within a unified linguistic interface, representing an important extension of multimodal large language models (MLLMs). Existing approaches predominantly rely on explicit geometric inputs: some leverage point clouds or reconstructed scenes, often augmented with rendered views, region-level alignments, or condensed 3D feature grids to support large-scale embodied training (Hong et al., 2023a; Chen et al., 2024b;c; Fu et al., 2024; Huang et al., 2023b); others map 3D features to the language space and model spatial relations to enable interactive dialogue (Huang et al., 2023a; 2024). Despite their progress, these methods invariably depend on complex inputs such as point clouds, reconstructed scenes, multi-view renderings, or object-level annotations, which impose substantial burdens on data acquisition, preprocessing, and computation, thereby limiting scalability and transferability.

**3D Reconstruction.** 3D reconstruction has evolved from multi-view geometry pipelines to neural implicit representations and, more recently, feed-forward transformer-based architectures. Classical methods yield accurate geometry but require dense views and heavy preprocessing (Schonberger & Frahm, 2016; Furukawa et al., 2015). Neural radiance fields and point-based extensions improve fidelity and efficiency but focus mainly on appearance modeling while lacking semantic reasoning (Mildenhall et al., 2021; Barron et al., 2022; Kerbl et al., 2023). Recent feed-forward approaches enable direct prediction of depth, pose, and point clouds from video inputs (Wang et al., 2024; Leroy et al., 2024; Wang et al., 2025a). Nevertheless, 3D reconstruction is still only weakly integrated into vision–language research, and its role in supporting semantic reasoning remains underexplored.

**Geometry Priors in Vision-Language Models.** Incorporating geometry priors has become a key approach for Vision-Language Models (VLMs) to enhance spatial understanding. Along a spectrum of reliance on explicit 3D inputs, existing methods can be organized into three categories: first, explicit input injection, which introduces depth, point clouds, or scene graphs as additional modalities to provide metric properties (Cai et al., 2025; Cheng et al., 2024b; Guo et al., 2023); second, internalization at the data and training level, which leverages spatially annotated corpora or geometric distillation to embed geometry implicitly into the alignment space, enabling spatial reasoning without explicit 3D inputs at inference (Chen et al., 2024a; Peng et al., 2023); and third, modular or prompt-based integration, which augments VLMs with lightweight modules or outputs from 3D foundation models, typically without large-scale retraining (Ma et al., 2024; Kerr et al., 2023). In contrast, our approach generates geometry through a video-driven reconstruction branch and achieves alignment with the semantic branch, enabling a structured and reusable integration of geometry priors within a video-based setting.

### 3 METHOD

We present Vid-LLM, a video-based 3D multimodal large language model (3D-MLLM). The main components are presented in the following sections: the Cross-Task adapter is described in Section 3.1, the reconstruction and reasoning branches are detailed in Sections 3.2 and 3.3, and the training strategy is outlined in Section 3.4. The overall architecture is shown in Fig. 2.

#### 3.1 CROSS-TASK ADAPTER

In Vid-LLM, we employ DINOv2 as the shared visual encoder to extract base tokens  $T_{base} \in \mathbb{R}^{N \times C}$  from the input image sequence, where  $N$  denotes the number of tokens and  $C$  is the embedding dimension. To enhance feature effectiveness, we introduce a Cross-Task adapter (CTA) that aligns 3D geometry priors with vision–language (VL) representations, facilitating the integration of geometric cues into multimodal reasoning.

To adapt the shared visual representations for different branches, we employ two lightweight MLP projection heads,  $\phi_{geom}(\cdot)$  and  $\phi_{lang}(\cdot)$ , which map the shared vision tokens to geometry-specific and semantic feature spaces, respectively:

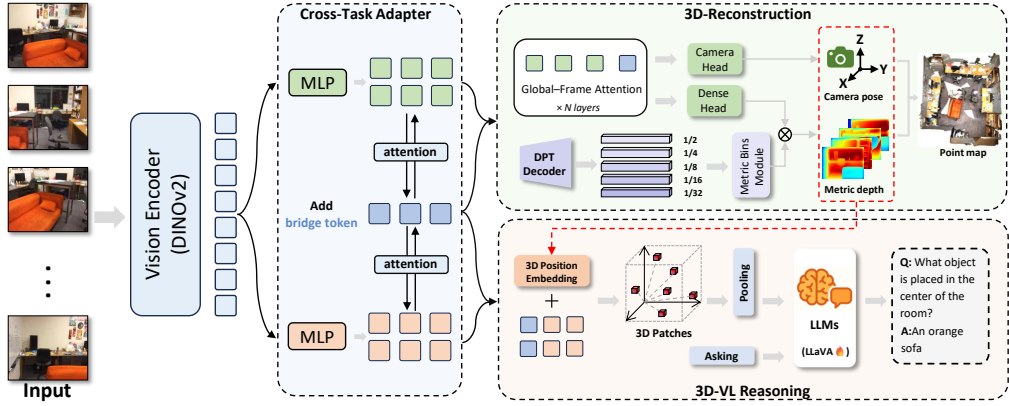


Figure 2: **Architecture of Vid-LLM.** From video, a shared DINOv2 encoder produces tokens that are bidirectionally fused by Cross-Task adapter with learnable Bridge Tokens, yielding geometric and semantic streams. The reconstruction branch predicts camera poses, depth and recovers real-scale via a Metric-Bins module, while the 3D-VL branch lifts features into 3D tokens for LLM reasoning.

$$T_{geom} = \phi_{geom}(T_{base}), \quad T_{lang} = \phi_{lang}(T_{base}) \quad (1)$$

To effectively align 3D geometry priors with vision–language representations thus enhance the integration of spatial cues into multimodal reasoning, we introduce learnable Bridge Tokens, denoted as  $T_{bridge} \in \mathbb{R}^{K \times C}$ . Acting as shared memory units, the bridge tokens attend to geometric and semantic features separately, and the updated representation is formulated as:

$$T'_{bridge} = \text{Attn}(T_{bridge}, T_{geom}^{fused}, T_{geom}^{fused}) + \text{Attn}(T_{bridge}, T_{lang}^{fused}, T_{lang}^{fused}) \quad (2)$$

where  $\text{Attn}(\cdot)$  denotes a standard multi-head attention operation. This operation enables bridge tokens to dynamically capture complementary information from both tasks and update their representations during training. The joint propagation of geometric and semantic signals strengthens the alignment of 3D geometry priors with vision–language features, leading to more robust cross-modal representations.

Finally, the updated bridge tokens  $T'_{bridge}$  are integrated into the feature streams, yielding enhanced task-specific representations  $T'_{geom}$  and  $T'_{lang}$ . These enriched features capture complementary geometric and semantic cues and are subsequently passed to the reconstruction and reasoning branches. In essence, the Cross-Task adapter establishes intrinsic geometry–semantics interaction at the feature level, allowing the two streams to reinforce and guide each other for more robust representations.

### 3.2 3D RECONSTRUCTION MODEL

In the reconstruction branch of Vid-LLM, we build on recent transformer-based architectures for end-to-end 3D reconstruction (Wang et al., 2025a) to recover scene geometry from video inputs. To additionally recover real-scale information, we design a Metric Depth Model that provides robust global scale cues, enabling reconstructions with both fine structural details and metric consistency.

**Geometry Encoding and Prediction Heads.** Based on the cross-task enhanced geometric features  $T'_{geom}$ , together with camera tokens  $T_{cam}$  and register tokens  $T_{reg}$ , the Global-Frame Attention backbone produces an integrated geometric representation, which is then fed into two prediction heads: a camera head estimating intrinsic-extrinsic parameters and a DPT head that predicts the relative depth map  $\hat{D}_{rel} \in \mathbb{R}^{H \times W}$ , where  $H$  and  $W$  denote the image height and width, respectively.

**Metric Depth Model.** To recover real-scale geometry, we equip the DINOv2 features with a DPT-style decoder that produces multi-scale depth representations. Each pixel’s depth is modeled using a bin-based formulation, where the probability  $p_i(k)$  over the  $k$  – th bin and its refined center  $c_i(k)$  jointly determine the prediction as  $\hat{d}(i) = \sum_{k=1}^N p_i(k) c_i(k)$ . we use an ordinal-aware normalization

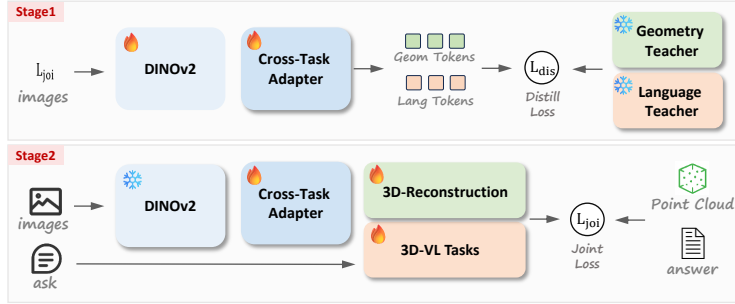


Figure 3: **Overview of the two-stage training strategy.** Stage-1 employs dual-teacher distillation to align geometry and semantics, and Stage-2 jointly optimizes reconstruction and 3D vision–language tasks.

to capture relative depth ordering. To further stabilize scale, the bin centers  $c_i(k)$  are adaptively refined as  $c_i(k) = c_k + \Delta c_i(k)$ , where  $\Delta c_i(k) = r_k(F_i)$  is predicted from the decoder features  $F_i$ . The resulting metric depth map  $\hat{D}_{\text{metric}} = \{\hat{d}(i)\}_{i=1}^{H \times W}$  provides global scale cues that are aligned with relative predictions for real-scale reconstruction.

**Real-Scale Alignment.** We estimate a scaling factor between the relative depth  $\hat{D}_{\text{rel}}$  predicted by the DPT head and the metric depth  $\hat{D}_{\text{metric}}$  predicted by the Metric Depth Model via weighted least squares. For each scene, 16 images are randomly sampled to compute per-image scaling factors, and their median is taken median as the final scene-level factor. This factor is then applied to convert both the relative depth and the predicted camera pose into real-world units. Rather than directly using metric depth as the final output, we adopt this alignment strategy since the DPT head provides more accurate texture details compared with the Metric Depth Model, which could also be observed from experimental results.

### 3.3 3D VISION–LANGUAGE MODEL

In the reasoning branch of Vid-LLM, cross-task-enhanced semantic features  $T'_{\text{lang}}$  are combined with reconstructed geometry to generate dense 3D patch representations, which are then fed into the LLM for 3D question answering, grounding, and captioning tasks.

**3D Patch Construction.** Each 2D feature  $T'_{\text{lang}}(i, j)$  is back-projected into 3D using the estimated depth  $\hat{D}$ , camera pose  $(\hat{R}, \hat{t})$  and intrinsics  $K$  produced by the 3D Reconstruction Model, yielding its camera-frame coordinates  $P_v(i, j)$  as:

$$P_v(i, j) = \hat{R}^{-1} K^{-1} [i, j, 1]^\top \hat{D}(i, j) - \hat{R}^{-1} \hat{t} \quad (3)$$

These coordinates are encoded by an MLP into positional embeddings  $P'_v(i, j)$  that match the dimensionality of the semantic features. Therefore, the final 3D patch tokens are then obtained by fusing geometry and semantic features:

$$T_{3D}(i, j) = T'_{\text{lang}}(i, j) + P'_v(i, j) \quad (4)$$

This operation feeds spatial information into the semantic tokens, further enhancing the spatial awareness in the LLM.

### 3.4 TRAINING STRATEGY

We adopt a two-stage training strategy to utilize the shared encoder for both geometry and semantics. Stage 1 performs dual-teacher distillation, transferring geometric priors from a reconstruction model and semantic knowledge from a multimodal LLM, enabling the encoder to learn both capabilities in a balanced way. Stage 2 jointly optimizes all downstream modules with 3D vision–language objectives, while incorporating auxiliary reconstruction losses to provide the model with sufficient reconstruction capability and ensure real-scale consistency. The overall pipeline is illustrated in Fig. 3.

**Stage-1 Dual-Teacher Distillation.** In stage 1, we adopt a dual-teacher distillation strategy to jointly train the DINO encoder and the Cross-Task adapter, enabling the modules to quickly learn both geometric and semantic representations. The pretrained DINO encoder and CLIP encoder serve as the geometry and semantic teachers in the distillation strategy, which are initialized from VGGT (Wang et al., 2025a) and LLaVA-3D (Zhu et al., 2025), respectively. The distillation loss is defined as:

$$L_{\text{distill}} = L_{\text{geo}}^{\text{feat}} + L_{\text{lang}}^{\text{feat}} + \lambda L_{\text{sc}} \quad (5)$$

where  $L_{\text{geo}}^{\text{feat}}$ ,  $L_{\text{lang}}^{\text{feat}}$  and  $L_{\text{sc}}$  are the geometry loss, semantic loss and structural consistency loss, respectively.  $\lambda$  is a balancing hyperparameter. The geometry loss and semantic loss are defined as:

$$L_{\text{geo}}^{\text{feat}} = \frac{1}{N} \sum_{i=1}^N \|\text{Norm}(T'_{\text{geom},i}) - \text{Norm}(T_{\text{tea},i}^{\text{geo}})\|_2^2, \quad L_{\text{lang}}^{\text{feat}} = 1 - \cos(T'_{\text{lang}}, T_{\text{tea}}^{\text{lang}}) \quad (6)$$

where  $T'_{\text{geom}}$  and  $T'_{\text{lang}}$  are the task-specific geometric and semantic features, respectively, extracted by the Cross-Task Adapter, serving as the student representations in the distillation strategy.  $T_{\text{tea}}^{\text{geo}}$  and  $T_{\text{tea}}^{\text{lang}}$  are the features of the DINO and CLIP encoder and serve as the teacher representations.  $N$  denotes the number of feature tokens sampled for alignment. To maintain structural consistency, we also introduce the structural consistency loss  $L_{\text{sc}}$ , which is defined as:

$$L_{\text{sc}} = \frac{1}{M^2} \|S_{\text{stu}} - S_{\text{tea}}\|_F^2, \quad \text{where } S_{\text{stu}} = Z_{\text{stu}} Z_{\text{stu}}^\top, S_{\text{tea}} = Z_{\text{tea}} Z_{\text{tea}}^\top \quad (7)$$

$Z_{\text{stu}} = [\text{Norm}(T'_{\text{geom}}); \text{Norm}(T'_{\text{lang}})] \in \mathbb{R}^{M \times C}$  concatenates the geometry and semantic tokens from student representation.  $Z_{\text{tea}} = [\text{Norm}(T_{\text{tea}}^{\text{geo}}); \text{Norm}(T_{\text{tea}}^{\text{lang}})]$  is similarly defined for the teacher representation.  $\|\cdot\|_F$  is the Frobenius norm, and  $M$  is the total number of tokens.

**Stage-2 Joint Optimization.** In Stage 2, we further fine-tune all the modules to optimize overall performance. The joint loss is defined as:

$$L_{\text{joint}} = L_{\text{recon-task}} + L_{\text{VL-task}} + L_{\text{MD}} \quad (8)$$

where  $L_{\text{recon-task}}$  is the multi-task loss for 3D reconstruction, consisting of the camera loss, depth loss, and point map loss following Wang et al. (2025a).  $L_{\text{VL-task}}$  supervises 3D vision–language reasoning, including cross-entropy loss for instruction-following tasks, along with bounding box regression and matching losses for grounding (Zhu et al. (2025)).  $L_{\text{MD}}$  represents the metric depth loss, combining a global scale penalty and a robust local refinement term, and is defined as:

$$L_{\text{MD}} = b^2 + \frac{1}{K} \sum_{i=1}^K \frac{(e_i - b)^2}{1 + \alpha|e_i - b|}, \quad (9)$$

where  $e_i = \log(d_i^{\text{pred}} + \varepsilon) - \log(d_i^{\text{gt}} + \varepsilon)$  is the log-depth error where  $\varepsilon$  is a small constant for numerical stability.  $b = \frac{1}{K} \sum_{i=1}^K e_i$  is the mean error across all  $K$  valid pixels in the image. The parameter  $\alpha > 0$  controls the robustness by down-weighting large residuals.

## 4 EXPERIMENTS

This section provides a comprehensive evaluation of Vid-LLM. In Section 4.1, the model is benchmarked on 3D vision–language reasoning tasks against state-of-the-art methods. In Section 4.2, the comparison with naive concatenation pipelines highlighting the importance of feature-level integration over post-hoc combination. In Section 4.3, ablation studies analyze the contributions of core modules. Further implementation details are provided in Appendix A.3.

### 4.1 3D VISION–LANGUAGE REASONING

**Overview.** To comprehensively assess the performance of Vid-LLM on 3D vision–language reasoning tasks, we conduct experiments using widely adopted datasets covering three task categories: 3D Question Answering on ScanQA (Azuma et al., 2022) and SQA3D (Ma et al., 2022), 3D Dense Captioning on Scan2Cap (Chen et al., 2021), and 3D Visual Grounding on ScanRefer (Chen et al.,

**Table 1: Evaluation of 3D Question Answering on ScanQA and SQA3D.** Methods marked with \* are 3D MLLM evaluated in video mode. “C” stands for “CIDEr”, “B-4” for “BLEU-4”, “M” for “METEOR”, “R” for “ROUGE”, and “EM@1” for top-1 exact match.

Method	ScanQA					SQA3D EM@1↑
	C↑	B-4↑	M↑	R↑	EM@1↑	
<i>3D-based models</i>						
Scan2Cap	—	—	—	—	—	41.0
ScanQA	64.9	10.1	13.1	33.3	21.1	47.2
3D-VisTA	69.6	10.4	13.9	35.7	22.4	48.5
3D-LLM	69.4	12.0	14.5	35.7	20.5	—
LL3DA	76.8	13.5	15.9	37.3	—	—
Grounded3D-LLM	75.9	13.2	—	—	—	—
Chat-3D v2	77.1	7.3	16.1	40.1	21.1	—
Scene-LLM	80.0	12.0	16.6	40.0	27.2	54.2
ChatScene	87.7	14.3	18.0	41.6	21.6	54.6
LEO	101.4	13.2	<b>20.0</b>	<b>49.2</b>	24.5	50.0
<i>Video-based models</i>						
VILA-40B	48.2	9.9	11.4	27.3	17.2	37.2
IXC-2.5-7B	53.9	8.7	13.2	31.5	19.4	41.5
LLaVA-OV-7B	78.2	13.3	17.2	40.5	22.9	47.6
LLaVA-Video-7B	88.7	—	—	—	—	48.5
Uni3DR2*	70.3	12.2	14.9	36.3	17.3	—
ChatScene*	85.6	—	—	—	—	52.9
Vid-LLM (Ours)	<b>101.9</b>	<b>15.8</b>	<b>18.3</b>	<b>49.5</b>	<b>27.6</b>	<b>57.3</b>

**Table 2: Evaluation of 3D Dense Captioning on Scan2Cap.** The n-gram metrics for Scan2Cap are governed by IoU@0.5.

Method	Scan2Cap			
	C@0.5↑	B-4@0.5↑	M@0.5↑	R@0.5↑
Scan2Cap	39.1	23.3	22.0	44.8
3D-VisTA	61.6	34.1	26.8	55.0
LL3DA	65.2	36.8	26.0	55.0
Grounded3D-LLM	70.2	35.0	—	—
LEO	68.4	<b>36.9</b>	27.7	57.8
ChatScene	<b>77.1</b>	36.3	<b>28.0</b>	<b>58.1</b>
Vid-LLM (Ours)	<b>81.5</b>	<b>40.6</b>	<b>28.7</b>	<b>61.8</b>

**Table 3: Evaluation of 3D Visual Grounding on ScanRefer and Multi3DRefer.**

Method	ScanRefer		Multi3DRefer	
	Acc@0.25↑	Acc@0.5↑	Acc@0.25↑	Acc@0.5↑
ScanRefer	37.3	24.3	—	—
3D-VisTA	<b>50.6</b>	45.5	—	—
3D-LLM	30.3	—	—	—
Chat-3D v2	35.9	30.4	—	—
Grounded3D-LLM	48.6	44.0	44.7	40.8
ChatScene	<b>55.5</b>	<b>50.2</b>	<b>57.1</b>	<b>52.4</b>
Vid-LLM (Ours)	50.1	46.7	47.2	42.9

2020), Multi3DRefer (Zhang et al., 2023), and Nr3D/Sr3D (Achlioptas et al., 2020b). We follow the standard evaluation protocols and metrics defined for each dataset. For grounding tasks, Vid-LLM directly outputs 3D bounding boxes on ScanRefer and Multi3DRefer, which target scene-level grounding with natural language descriptions. For Nr3D/Sr3D, we adopt the Chat-3D v2 protocol (Huang et al., 2023a), which employs the ViL3DRel (Chen et al., 2022) method to generate grounding candidates, emphasizing instance-level referential resolution.

**Baseline.** For the 3D Question Answering and 3D Dense Captioning tasks, we compare Vid-LLM against representative 3D vision–language reasoning models. The comparison methods include: ScanQA (Azuma et al., 2022), Scan2Cap (Chen et al., 2021), 3D-VisTA (Zhu et al., 2023), 3D-LLM (Hong et al., 2023b), LL3DA (Chen et al., 2024b), Grounded3D-LLM (Chen et al., 2024c), Chat-3D v2 (Huang et al., 2023a), LEO (Huang et al., 2023b), Scene-LLM (Fu et al., 2024), and ChatScene (Huang et al., 2024). All these methods rely on explicit 3D scene inputs. We also compare recent video-based approaches, namely VILA-40B (Lin et al., 2024), IXC-2.5-7B (Zhang et al., 2024b), LLaVA-OV-7B (Li et al., 2024), LLaVA-Video-7B (LLaVA Team, 2024), and Uni3DR2 (Chu et al., 2024). For the 3D visual grounding benchmarks, we compare Vid-LLM with task-specific grounding models including ScanRefer (Chen et al., 2020), 3D-VisTA (Zhu et al., 2023), ReferIt3D (Achlioptas et al., 2020a), 3DVG-Trans (Zhao et al., 2021), MVT (Huang et al., 2022), ViL3DRel (Chen et al., 2022), and SceneVerse (Jia et al., 2024). We also compare against recent 3D-MLLMs capable of performing grounding tasks, including 3D-LLM (Hong et al., 2023a), Chat-3D v2 (Huang et al., 2023a), Grounded3D-LLM (Chen et al., 2024c), and ChatScene (Huang et al., 2024). These comparisons collectively provide a comprehensive evaluation of our proposed method for 3D vision–language (VL) reasoning.

**Result & Analysis.** From Tab. 1, we can observe that Vid-LLM achieves the best performance in almost all metrics on the 3D Question Answering benchmarks, which verifies the effectiveness of our proposed method. Compared with 3D-based models and 2D-based models, our method achieves an average improvement of 9% and 31% over the second-best results, respectively. This illustrates that the integration of geometric cues into semantic reasoning can significantly improve perception performance. Furthermore, we also carried out experiments on the 3D Dense Captioning and 3D visual grounding task, which can be seen in Tab. 2 and Tab. 3. Benefiting from our designed cross-task adapter that compactly integrates semantic and geometric information, our method demonstrates superior multi-task capabilities. It is worth noting that in Tab. 3, our method ranks second to ChatScene. This is because ChatScene employs point cloud inputs with instance segmentation, which require much higher acquisition cost than the video inputs used in our model. For qualitative



Figure 4: **Qualitative results of 3D visual grounding on the ScanRefer dataset.** The predicted 3D bounding boxes are visualized on point clouds reconstructed by our model.

Table 4: **Evaluation of 3D Visual Grounding on Nr3D and Sr3D.** Results are reported in grounding accuracy (%).

Method	Nr3D			Sr3D		
	Overall↑	Hard↑	View Dep↑	Overall↑	Hard↑	View Dep↑
ScanRefer	34.2	23.5	29.9	—	—	—
ReferIT3D	35.6	27.9	32.5	40.8	31.5	39.2
3DVG-Trans	40.8	34.8	34.8	51.4	44.9	44.6
MVT	55.1	49.1	54.3	64.5	58.8	58.4
Vil3DRel	62.6	55.6	59.8	72.5	68.1	58.0
Chat-3D v2	63.6	57.0	61.1	73.1	68.4	58.1
3D-VisTA	64.2	56.7	61.5	76.4	71.3	58.9
SceneVerse	64.9	57.8	56.9	77.5	71.6	62.8
Vid-LLM (Ours)	<b>65.4</b>	<b>57.9</b>	<b>61.9</b>	<b>77.8</b>	<b>72.2</b>	<b>63.1</b>

Table 5: **Comparison with Naive Concatenation on Reconstruction, 3D VL, and Efficiency.** The reported metrics are averaged over all evaluation scores on ScanNet and ScanQA. Reconstruction is evaluated without scale normalization.

Method	Recon	3D VL Tasks	Time (s / scene) ↓
	ScanNet ↑	ScanQA ↑	
VGGT+LLaVA3D	—	24.6	2.7s
VGGT+real-scale+LLaVA-3D	0.587	40.3	2.7s
VGGT+real-scale+LLaVA-3D*	0.587	39.1	2.7s
VGGT*+real-scale+LLaVA-3D	0.591	42.1	2.7s
VGGT*+real-scale+LLaVA-3D*	0.591	41.6	2.7s
Vid-LLM (Ours)	0.582	<b>45.7</b>	<b>1.6s</b>

analysis, we visualize the 3D grounding on the SCanRefer dataset in Fig. 4. The results intuitively illustrates the predictive capability of 3D grounding in typical scenarios.

#### 4.2 COMPARISON WITH NAIVE CONCATENATION

**Overview.** To examine whether video-based 3D vision-language (3D VL) tasks can be addressed by directly combining a reconstruction model with a 3D multimodal LLM, we build a concatenation baseline by feeding the 3D reconstruction results from VGGT (Wang et al., 2025a) into the reasoning model LLaVA-3D (Zhu et al., 2025), since our reconstruction backbone is derived from VGGT and our reasoning branch is based on LLaVA-3D. For a fair comparison, we consider several baseline formulations. First, because the raw outputs of VGGT do not preserve metric scale, we additionally evaluate settings where its predictions are aligned with metric scale before being passed to LLaVA-3D. Second, since our Vid-LLM is fine-tuned on ScanNet and its 3D-LLM module is further fine-tuned on predicted 3D scenes, we correspondingly fine-tune VGGT on ScanNet (denoted VGGT\*) and take the point clouds produced by both VGGT and VGGT as geometric supervision to fine-tune LLaVA-3D (denoted LLaVA-3D\*).

**Result & Analysis.** As shown in Tab. 5, compared with other settings that incorporate metric-scale alignment, the direct concatenation of VGGT with LLaVA-3D is largely ineffective for 3D VL tasks, highlighting that the absence of metric-scale cues renders geometric representations inadequate for reasoning. With metric-scale alignment, the 3D VL score increases substantially from 24.6 to 40.3, demonstrating the necessity of metric-scale alignment. A further comparison between VGGT and VGGT\* shows that fine-tuning VGGT on ScanNet improves the reconstruction metric from 0.587 to 0.591. This improvement in geometric accuracy also leads to a higher 3D VL score, increasing from 40.3 to 42.1. However, when LLaVA-3D is further fine-tuned using predicted point clouds as geometric supervision, the 3D VL score decreases (42.1 → 41.6), suggesting that direct supervision from predicted geometry can introduce geometric bias and weaken semantic consistency. Finally, a comparison of VGGT\*+LLaVA-3D\* with our Vid-LLM highlights the main advantage of our approach: Vid-LLM achieves a notable improvement in 3D VL reasoning (45.7 vs. 42.1) while also reducing inference time (1.6s vs. 2.7s). It is worth noticing that the reconstruction metric of our method is slightly lower than the best baseline, this is because our model prioritizes geometry-semantics interaction over raw geometric accuracy. Our advantage derives from the compact design

Table 6: **Ablation on Cross-Task adapter (CTA) and Metric Depth (MD) Modules.** Results are reported as the mean of evaluation metrics across the corresponding datasets.

	3D VL Tasks			3D Recon
	ScanOA $\uparrow$	Scan2Cap $\uparrow$	ScanRefer $\uparrow$	scannet $\uparrow$
w/o-CTA	33.7	36.6	34.1	0.402
CTA -w/o Bridge	40.8	45.6	42.2	0.473
CTA -4tokens	43.8	50.9	47.8	0.501
CTA -8tokens	44.1	52.7	48.1	0.529
CTA -16tokens (Ours)	<b>45.7</b>	<b>53.2</b>	<b>48.4</b>	<b>0.582</b>
CTA -32tokens	45.2	52.8	47.6	0.564
w/o MD	29.6	35.7	33.9	-
MD - w/o Alignment	42.1	49.6	43.2	0.531
MD (Ours)	<b>45.7</b>	<b>53.2</b>	<b>48.4</b>	<b>0.582</b>

and the Cross-Task Adapter, which aligns 3D geometry priors with vision-language representations and provides geometric constraints that improve the robustness of reasoning under geometric uncertainty. By facilitating effective geometry–semantics interaction, CTA ensures that Vid-LLM maintains strong reasoning performance even without relying on precise external 3D inputs. Further analysis of our model’s reconstruction performance can be found in Appendix A.2.

#### 4.3 ABLATION STUDIES

**Cross-Task adapter.** As shown in Tab. 6, we conduct ablation studies on the Cross-Task adapter to examine its role in video-based 3D MLLM. Since 3D VL reasoning relies on 3D scene information provided by geometric reconstruction, both tasks must be jointly optimized to achieve strong performance. Without CTA, neither reconstruction nor reasoning performs well, revealing that a single visual feature representation is insufficient to serve both tasks simultaneously. Introducing CTA brings significant improvements to both reconstruction and reasoning by facilitating cross-task feature interaction. However, without bridge tokens, the adapter cannot effectively align geometry priors with semantic features, resulting in notably weaker performance. Adding bridge tokens leads to significant gains, and using 16 tokens achieves the best trade-off between accuracy and model complexity by ensuring sufficient interaction without redundancy.

**Metric Depth Modules.** Tab. 6 also reports ablations on the use of metric depth and our alignment strategy. Without metric depth supervision (w/o MD), scale ambiguity destroys geometric consistency and leads to near failure of 3D VL reasoning. Incorporating metric depth without alignment (MD – w/o Alignment) preserves absolute scale but produces less accurate reconstruction, which in turn limits the performance of 3D VL tasks. By contrast, combining metric depth with our scale alignment strategy effectively exploits both global scale cues and relative structural details, yielding the most accurate reconstruction and consistently stronger results on 3D VL tasks.

**Two-Stage Training.** Fig. 5 compares different training strategies to assess their impact on convergence and performance. The single-stage setting converges slowly and stabilizes at a relatively high loss value, reflecting gradient interference when all modules are trained jointly. The two-stage strategy with a single teacher offers limited supervisory signals, limiting optimization quality. Removing the relational loss also degrades convergence and accuracy, highlighting the importance of cross-task consistency. In contrast, our two-stage strategy converges fastest and achieves the lowest final loss.

## 5 CONCLUSION

In this work, we present Vid-LLM, a video-based 3D Multimodal Large Language Model (3D-MLLM). Our compact architecture extracts geometric cues from video and feeds them into the LLM through a 3D patch construction strategy to accomplish spatial reasoning. A central component of our framework is the Cross-Task adapter that aligns 3D geometry priors with vision–language representations. This design enhances their integration into the MLLM and improves the robustness of reasoning under uncertain geometry. Together with a two-stage training strategy, our model achieves

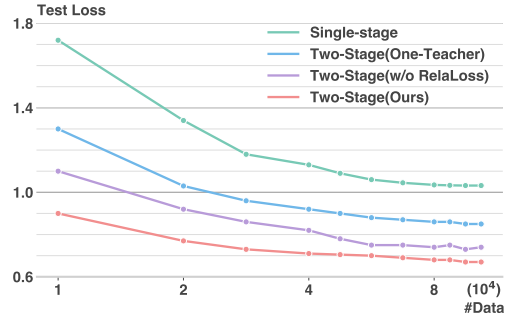


Figure 5: Test loss vs. data size across training strategies.

greater training stability and faster convergence. Extensive experiments on 3D vision–language benchmarks demonstrate that Vid-LLM achieves state-of-the-art results on several benchmarks and remains competitive on the others, while ablation studies validate the effectiveness of each component.

## 6 REPRODUCIBILITY STATEMENT

We are committed to ensuring reproducibility. Part of our implementation is provided in the Supplementary Materials. Upon acceptance, we will release the complete code, datasets, and pretrained checkpoints to enable full verification of our results.

## REFERENCES

Panos Achlioptas, Ahmed Abdelreheem, Fei Xia, Mohamed Elhoseiny, and Leonidas Guibas. Referit3d: Neural listeners for fine-grained 3d object identification in real-world scenes. In *European conference on computer vision*, pp. 422–440. Springer, 2020a.

Panos Achlioptas, Ahmed Abdelreheem, Fei Xia, Mohamed Elhoseiny, and Leonidas Guibas. Referit3d: Neural listeners for fine-grained 3d object identification in real-world scenes. In *European conference on computer vision*, pp. 422–440. Springer, 2020b.

Daichi Azuma, Taiki Miyanishi, Shuhei Kurita, and Motoaki Kawanabe. Scanqa: 3d question answering for spatial scene understanding. In *proceedings of the IEEE/CVF conference on computer vision and pattern recognition*, pp. 19129–19139, 2022.

Jonathan T Barron, Ben Mildenhall, Dor Verbin, Pratul P Srinivasan, and Peter Hedman. Mip-nerf 360: Unbounded anti-aliased neural radiance fields. In *Proceedings of the IEEE/CVF conference on computer vision and pattern recognition*, pp. 5470–5479, 2022.

Shariq Farooq Bhat, Reiner Birk, Diana Wofk, Peter Wonka, and Matthias Müller. Zoedepth: Zero-shot transfer by combining relative and metric depth. *arXiv preprint arXiv:2302.12288*, 2023.

Wenxiao Cai, Iaroslav Ponomarenko, Jianhao Yuan, Xiaoqi Li, Wankou Yang, Hao Dong, and Bo Zhao. Spatialbot: Precise spatial understanding with vision language models. In *2025 IEEE International Conference on Robotics and Automation (ICRA)*, pp. 9490–9498. IEEE, 2025.

Boyuan Chen, Zhuo Xu, Sean Kirmani, Brain Ichter, Dorsa Sadigh, Leonidas Guibas, and Fei Xia. Spatialvilm: Endowing vision-language models with spatial reasoning capabilities. In *Proceedings of the IEEE/CVF Conference on Computer Vision and Pattern Recognition*, pp. 14455–14465, 2024a.

Dave Zhenyu Chen, Angel X Chang, and Matthias Nießner. Scanrefer: 3d object localization in rgbd scans using natural language. In *European conference on computer vision*, pp. 202–221. Springer, 2020.

Shizhe Chen, Pierre-Louis Guhur, Makarand Tapaswi, Cordelia Schmid, and Ivan Laptev. Language conditioned spatial relation reasoning for 3d object grounding. *Advances in neural information processing systems*, 35:20522–20535, 2022.

Sijin Chen, Xin Chen, Chi Zhang, Mingsheng Li, Gang Yu, Hao Fei, Hongyuan Zhu, Jiayuan Fan, and Tao Chen. Ll3da: Visual interactive instruction tuning for omni-3d understanding reasoning and planning. In *Proceedings of the IEEE/CVF conference on computer vision and pattern recognition*, pp. 26428–26438, 2024b.

Yilun Chen, Shuai Yang, Haifeng Huang, Tai Wang, Runsen Xu, Ruiyuan Lyu, Dahua Lin, and Jiangmiao Pang. Grounded 3d-llm with referent tokens. *arXiv preprint arXiv:2405.10370*, 2024c.

Zhenyu Chen, Ali Gholami, Matthias Nießner, and Angel X Chang. Scan2cap: Context-aware dense captioning in rgbd scans. In *Proceedings of the IEEE/CVF conference on computer vision and pattern recognition*, pp. 3193–3203, 2021.

An-Chieh Cheng, Hongxu Yin, Yang Fu, Qiushan Guo, Ruihan Yang, Jan Kautz, Xiaolong Wang, and Sifei Liu. Spatialrgpt: Grounded spatial reasoning in vision-language models. *Advances in Neural Information Processing Systems*, 37:135062–135093, 2024a.

An-Chieh Cheng, Hongxu Yin, Yang Fu, Qiushan Guo, Ruihan Yang, Jan Kautz, Xiaolong Wang, and Sifei Liu. Spatialrgpt: Grounded spatial reasoning in vision-language models. *Advances in Neural Information Processing Systems*, 37:135062–135093, 2024b.

Tao Chu, Pan Zhang, Xiaoyi Dong, Yuhang Zang, Qiong Liu, and Jiaqi Wang. Unified scene representation and reconstruction for 3d large language models. *arXiv preprint arXiv:2404.13044*, 2024.

Angela Dai, Angel X Chang, Manolis Savva, Maciej Halber, Thomas Funkhouser, and Matthias Nießner. Scannet: Richly-annotated 3d reconstructions of indoor scenes. In *Proceedings of the IEEE conference on computer vision and pattern recognition*, pp. 5828–5839, 2017.

Rao Fu, Jingyu Liu, Xilun Chen, Yixin Nie, and Wenhan Xiong. Scene-llm: Extending language model for 3d visual understanding and reasoning. *arXiv preprint arXiv:2403.11401*, 2024.

Yasutaka Furukawa, Carlos Hernández, et al. Multi-view stereo: A tutorial. *Foundations and trends® in Computer Graphics and Vision*, 9(1-2):1–148, 2015.

Ziyu Guo, Renrui Zhang, Xiangyang Zhu, Yiwen Tang, Xianzheng Ma, Jiaming Han, Kexin Chen, Peng Gao, Xianzhi Li, Hongsheng Li, et al. Point-bind & point-llm: Aligning point cloud with multi-modality for 3d understanding, generation, and instruction following. *arXiv preprint arXiv:2309.00615*, 2023.

Huy Ha and Shuran Song. Semantic abstraction: Open-world 3d scene understanding from 2d vision-language models. *arXiv preprint arXiv:2207.11514*, 2022.

Yining Hong, Haoyu Zhen, Peihao Chen, Shuhong Zheng, Yilun Du, Zhenfang Chen, and Chuang Gan. 3d-llm: Injecting the 3d world into large language models. *Advances in Neural Information Processing Systems*, 36:20482–20494, 2023a.

Yining Hong, Haoyu Zhen, Peihao Chen, Shuhong Zheng, Yilun Du, Zhenfang Chen, and Chuang Gan. 3d-llm: Injecting the 3d world into large language models. *Advances in Neural Information Processing Systems*, 36:20482–20494, 2023b.

Haifeng Huang, Zehan Wang, Rongjie Huang, Luping Liu, Xize Cheng, Yang Zhao, Tao Jin, and Zhou Zhao. Chat-3d v2: Bridging 3d scene and large language models with object identifiers. *CoRR*, 2023a.

Haifeng Huang, Yilun Chen, Zehan Wang, Rongjie Huang, Runsen Xu, Tai Wang, Luping Liu, Xize Cheng, Yang Zhao, Jiangmiao Pang, et al. Chat-scene: Bridging 3d scene and large language models with object identifiers. *Advances in Neural Information Processing Systems*, 37:113991–114017, 2024.

Jiangyong Huang, Silong Yong, Xiaojian Ma, Xiongkun Linghu, Puhao Li, Yan Wang, Qing Li, Song-Chun Zhu, Baoxiong Jia, and Siyuan Huang. An embodied generalist agent in 3d world. *arXiv preprint arXiv:2311.12871*, 2023b.

Shijia Huang, Yilun Chen, Jiaya Jia, and Liwei Wang. Multi-view transformer for 3d visual grounding. In *Proceedings of the IEEE/CVF Conference on Computer Vision and Pattern Recognition*, pp. 15524–15533, 2022.

Baoxiong Jia, Yixin Chen, Huangyue Yu, Yan Wang, Xuesong Niu, Tengyu Liu, Qing Li, and Siyuan Huang. Sceneverse: Scaling 3d vision-language learning for grounded scene understanding. In *European Conference on Computer Vision*, pp. 289–310. Springer, 2024.

Jihong Ju, Ching Wei Tseng, Oleksandr Bailo, Georgi Dikov, and Mohsen Ghafoorian. Dg-recon: Depth-guided neural 3d scene reconstruction. In *Proceedings of the IEEE/CVF International Conference on Computer Vision*, pp. 18184–18194, 2023.

Bernhard Kerbl, Georgios Kopanas, Thomas Leimkühler, and George Drettakis. 3d gaussian splatting for real-time radiance field rendering. *ACM Trans. Graph.*, 42(4):139–1, 2023.

Justin Kerr, Chung Min Kim, Ken Goldberg, Angjoo Kanazawa, and Matthew Tancik. Lerf: Language embedded radiance fields. In *Proceedings of the IEEE/CVF international conference on computer vision*, pp. 19729–19739, 2023.

Johannes Kopf, Xuejian Rong, Jia-Bin Huang, Kevin Matzen, et al. Robust consistent video depth estimation. In *Proceedings of the IEEE/CVF Conference on Computer Vision and Pattern Recognition (CVPR)*, 2021.

Seoyoung Lee and Joonseok Lee. Posediff: Pose-conditioned multimodal diffusion model for unbounded scene synthesis from sparse inputs. In *Proceedings of the IEEE/CVF Winter Conference on Applications of Computer Vision*, pp. 5007–5017, 2024.

Yao-Chih Lee, Kuan-Wei Tseng, Guan-Sheng Chen, and Chu-Song Chen. Globally consistent video depth and pose estimation with efficient test-time training. *arXiv preprint arXiv:2208.02709*, 2022.

Vincent Leroy, Yohann Cabon, and Jérôme Revaud. Grounding image matching in 3d with mast3r. In *European Conference on Computer Vision*, pp. 71–91. Springer, 2024.

Bo Li et al. Llava-onevision: Easy visual task transfer. *arXiv preprint arXiv:2408.03326*, 2024.

Ji Lin, Hongxu Yin, Wei Ping, Yao Lu, Pavlo Molchanov, Andrew Tao, Huizi Mao, Jan Kautz, Mohammad Shoeybi, and Song Han. Vila: On pre-training for visual language models. In *Proceedings of the IEEE/CVF Conference on Computer Vision and Pattern Recognition (CVPR)*, 2024.

Philipp Lindenberger, Paul-Edouard Sarlin, Viktor Larsson, and Marc Pollefeys. Pixel-perfect structure-from-motion with featuremetric refinement. In *Proceedings of the IEEE/CVF International Conference on Computer Vision (ICCV)*, 2021.

Liman Liu, Fenghao Zhang, Wanjuan Su, Yuhang Qi, and Wenbing Tao. Geometric prior-guided self-supervised learning for multi-view stereo. *Remote Sensing*, 15(8):2109, 2023. doi: 10.3390/rs15082109.

Ze Liu, Han Hu, Yutong Lin, Zhuliang Yao, Zhenda Xie, Yixuan Wei, Jia Ning, Yue Cao, Zheng Zhang, Li Dong, Furu Wei, and Baining Guo. Swin transformer v2: Scaling up capacity and resolution. In *Proceedings of the IEEE/CVF Conference on Computer Vision and Pattern Recognition (CVPR)*, pp. 12009–12019, 2022.

LLaVA Team. Llava-video: Video instruction tuning with synthetic data. *arXiv preprint arXiv:2410.02713*, 2024.

Chenyang Ma, Kai Lu, Ta-Ying Cheng, Niki Trigoni, and Andrew Markham. Spatialpin: Enhancing spatial reasoning capabilities of vision-language models through prompting and interacting 3d priors. *Advances in neural information processing systems*, 37:68803–68832, 2024.

Xiaojian Ma, Silong Yong, Zilong Zheng, Qing Li, Yitao Liang, Song-Chun Zhu, and Siyuan Huang. Sqa3d: Situated question answering in 3d scenes. *arXiv preprint arXiv:2210.07474*, 2022.

Ben Mildenhall, Pratul P Srinivasan, Matthew Tancik, Jonathan T Barron, Ravi Ramamoorthi, and Ren Ng. Nerf: Representing scenes as neural radiance fields for view synthesis. *Communications of the ACM*, 65(1):99–106, 2021.

Zak Murez, Tarrence van As, James Bartolozzi, Ayan Sinha, Vijay Badrinarayanan, and Andrew Rabinovich. Atlas: End-to-end 3d scene reconstruction from posed images. In *European Conference on Computer Vision (ECCV)*, 2020.

Humza Naveed, Asad Ullah Khan, Shi Qiu, Muhammad Saqib, Saeed Anwar, Muhammad Usman, Naveed Akhtar, Nick Barnes, and Ajmal Mian. A comprehensive overview of large language models. *ACM Transactions on Intelligent Systems and Technology*, 16(5):1–72, 2025.

Jia Ning, Chen Li, Zheng Zhang, Zigang Geng, Qi Dai, Kun He, and Han Hu. All in tokens: Unifying output space of visual tasks via soft token. In *Proceedings of the IEEE/CVF International Conference on Computer Vision (ICCV)*, 2023.

Mingyang Ou, Heng Li, Haofeng Liu, Xiaoxuan Wang, Chenlang Yi, Luoying Hao, Yan Hu, and Jiang Liu. Mvd-net: Semantic segmentation of cataract surgery using multi-view learning. In *2022 44th Annual International Conference of the IEEE Engineering in Medicine & Biology Society (EMBC)*, pp. 5035–5038. IEEE, 2022.

Vaishakh Patil, Christos Sakaridis, Alexander Liniger, and Luc Van Gool. P3depth: Monocular depth estimation with a piecewise planarity prior. In *Proceedings of the IEEE/CVF Conference on Computer Vision and Pattern Recognition (CVPR)*, 2022.

Songyou Peng, Kyle Genova, Chiyu Jiang, Andrea Tagliasacchi, Marc Pollefeys, Thomas Funkhouser, et al. Openscene: 3d scene understanding with open vocabularies. In *Proceedings of the IEEE/CVF conference on computer vision and pattern recognition*, pp. 815–824, 2023.

Alec Radford, Jeffrey Wu, Rewon Child, David Luan, Dario Amodei, Ilya Sutskever, et al. Language models are unsupervised multitask learners. *OpenAI blog*, 1(8):9, 2019.

René Ranftl, Alexey Bochkovskiy, and Vladlen Koltun. Vision transformers for dense prediction. In *Proceedings of the IEEE/CVF International Conference on Computer Vision (ICCV)*, pp. 12159–12168, 2021.

Jeremy Reizenstein, Roman Shapovalov, Philipp Henzler, Luca Sbordone, Patrick Labatut, and David Novotny. Common objects in 3d: Large-scale learning and evaluation of real-life 3d category reconstruction. In *Proceedings of the IEEE/CVF international conference on computer vision*, pp. 10901–10911, 2021.

Ruilong Ren, Xinyu Zhao, Weichen Xu, Jian Cao, Xinxin Xu, and Xing Zhang. A survey of language-grounded multimodal 3d scene understanding. *Knowledge-Based Systems*, pp. 113650, 2025.

Junha Roh, Karthik Desingh, Ali Farhadi, and Dieter Fox. Languageref: Spatial-language model for 3d visual grounding. In *Conference on Robot Learning*, pp. 1046–1056. PMLR, 2022.

Paul-Edouard Sarlin, Daniel DeTone, Tomasz Malisiewicz, and Andrew Rabinovich. SuperGlue: Learning feature matching with graph neural networks. In *Proceedings of the IEEE/CVF Conference on Computer Vision and Pattern Recognition (CVPR)*, pp. 4938–4947, 2020.

Johannes L Schonberger and Jan-Michael Frahm. Structure-from-motion revisited. In *Proceedings of the IEEE conference on computer vision and pattern recognition*, pp. 4104–4113, 2016.

Nathan Silberman, Derek Hoiem, Pushmeet Kohli, and Rob Fergus. Indoor segmentation and support inference from rgbd images. In *European conference on computer vision*, pp. 746–760. Springer, 2012.

Jiaming Sun, Yiming Xie, Linghao Chen, Xiaowei Zhou, and Hujun Bao. Neuralrecon: Real-time coherent 3d reconstruction from monocular video. In *Proceedings of the IEEE/CVF conference on computer vision and pattern recognition*, pp. 15598–15607, 2021.

Ashish Vaswani, Noam Shazeer, Niki Parmar, Jakob Uszkoreit, Llion Jones, Aidan N Gomez, Łukasz Kaiser, and Illia Polosukhin. Attention is all you need. *Advances in neural information processing systems*, 30, 2017.

Jianyuan Wang, Minghao Chen, Nikita Karaev, Andrea Vedaldi, Christian Rupprecht, and David Novotny. Vggt: Visual geometry grounded transformer. In *Proceedings of the Computer Vision and Pattern Recognition Conference*, pp. 5294–5306, 2025a.

Qianqian Wang, Yifei Zhang, Aleksander Holynski, Alexei A. Efros, and Angjoo Kanazawa. Continuous 3d perception model with persistent state. *arXiv preprint arXiv:2501.12387*, 2025b.

Shuzhe Wang, Vincent Leroy, Yohann Cabon, Boris Chidlovskii, and Jerome Revaud. Dust3r: Geometric 3d vision made easy. In *Proceedings of the IEEE/CVF Conference on Computer Vision and Pattern Recognition*, pp. 20697–20709, 2024.

Dong Wu, Zike Yan, and Hongbin Zha. Panorecon: Real-time panoptic 3d reconstruction from monocular video. In *Proceedings of the IEEE/CVF Conference on Computer Vision and Pattern Recognition*, pp. 21507–21518, 2024.

Jiayang Wu, Wensheng Gan, Zefeng Chen, Shicheng Wan, and Philip S Yu. Multimodal large language models: A survey. In *2023 IEEE International Conference on Big Data (BigData)*, pp. 2247–2256. IEEE, 2023.

Guangkai Xu, Wei Yin, Hao Chen, Chunhua Shen, Kai Cheng, and Feng Zhao. Frozenrecon: Pose-free 3d scene reconstruction with frozen depth models. In *2023 IEEE/CVF International Conference on Computer Vision (ICCV)*, pp. 9276–9286. IEEE, 2023.

Jianing Yang, Alexander Sax, Kevin J Liang, Mikael Henaff, Hao Tang, Ang Cao, Joyce Chai, Franziska Meier, and Matt Feiszli. Fast3r: Towards 3d reconstruction of 1000+ images in one forward pass. In *Proceedings of the Computer Vision and Pattern Recognition Conference*, pp. 21924–21935, 2025.

Lihe Yang, Bingyi Kang, Zilong Huang, Xiaogang Xu, Jiashi Feng, and Hengshuang Zhao. Depth anything: Unleashing the power of large-scale unlabeled data. In *Proceedings of the IEEE/CVF conference on computer vision and pattern recognition*, pp. 10371–10381, 2024.

Shukang Yin, Chaoyou Fu, Sirui Zhao, Ke Li, Xing Sun, Tong Xu, and Enhong Chen. A survey on multimodal large language models. *National Science Review*, 11(12):nwa403, 2024.

Duzhen Zhang, Yahan Yu, Jiahua Dong, Chenxing Li, Dan Su, Chenhui Chu, and Dong Yu. Mmlms: Recent advances in multimodal large language models. *arXiv preprint arXiv:2401.13601*, 2024a.

Pan Zhang, Xiaoyi Dong, Yuhang Zang, Yuhang Cao, Rui Qian, Lin Chen, Qipeng Guo, Haodong Duan, Bin Wang, Linke Ouyang, et al. Internlm-xcomposer-2.5: A versatile large vision language model supporting long-contextual input and output. *arXiv preprint arXiv:2407.03320*, 2024b.

Shangzhan Zhang, Jianyuan Wang, Yinghao Xu, Nan Xue, Christian Rupprecht, Xiaowei Zhou, Yujun Shen, and Gordon Wetzstein. Flare: Feed-forward geometry, appearance and camera estimation from uncalibrated sparse views. In *Proceedings of the IEEE/CVF Conference on Computer Vision and Pattern Recognition (CVPR)*, 2025.

Yiming Zhang, ZeMing Gong, and Angel X Chang. Multi3drefer: Grounding text description to multiple 3d objects. In *Proceedings of the IEEE/CVF International Conference on Computer Vision*, pp. 15225–15236, 2023.

Lichen Zhao, Daigang Cai, Lu Sheng, and Dong Xu. 3dvg-transformer: Relation modeling for visual grounding on point clouds. In *Proceedings of the IEEE/CVF International Conference on Computer Vision*, pp. 2928–2937, 2021.

Wenliang Zhao, Yongming Rao, Zuyan Liu, Benlin Liu, Jie Zhou, and Jiwen Lu. Unleashing text-to-image diffusion models for visual perception. In *Proceedings of the IEEE/CVF International Conference on Computer Vision (ICCV)*, 2023.

Tinghui Zhou, Richard Tucker, John Flynn, Graham Fyffe, and Noah Snavely. Stereo magnification: Learning view synthesis using multiplane images. *arXiv preprint arXiv:1805.09817*, 2018.

Chenming Zhu, Tai Wang, Wenwei Zhang, Jiangmiao Pang, and Xihui Liu. Llava-3d: A simple yet effective pathway to empowering lmms with 3d capabilities. In *International Conference on Computer Vision (ICCV)(19/10/2025-23/10/2025, Honolulu, Hawai'i)*, 2025.

Ziyu Zhu, Xiaojian Ma, Yixin Chen, Zhidong Deng, Siyuan Huang, and Qing Li. 3d-vista: Pre-trained transformer for 3d vision and text alignment. In *Proceedings of the IEEE/CVF International Conference on Computer Vision*, pp. 2911–2921, 2023.

## A APPENDIX

In the Appendix, we provide the following experimental results:

- qualitative visualizations of Vid-LLM outputs in Appendix A.1;
- supplementary experiments on reconstruction performance in Appendix A.2;
- comprehensive implementation details, covering optimization settings, training procedures, and hyperparameters in Appendix A.3.
- The Use of Large Language Models (LLMs) Statement in Appendix A.4.

### A.1 QUALITATIVE RESULTS

	Reconstruction	Question & Answer	Reconstruction	Question & Answer
3D Question Answering		<p><b>Q:</b> How many chairs are there in the room ?  <b>A:</b> Three.</p> <p><b>Q:</b> Where is the monitor?  <b>A:</b> In the corner of the desk against the wall.</p>		<p><b>Q:</b> Where is the bed in the room ?  <b>A:</b> On the right side of the room</p> <p><b>Q:</b> What color are the curtains.  <b>A:</b> Brown.</p>
3D Dense Captioning		<p><b>Q:</b> Describe the room in detail.  <b>A:</b> In the center of the meeting room, there is a light-colored conference table, surrounded by black conference chairs...</p>		<p><b>Q:</b> Describe the Washbasin in detail.  <b>A:</b> This is a brown washbasin, made entirely of light brown wood, with a circular washbasin in the center of the wash...</p>
3D Visual Grounding		<p><b>Q:</b> There are two beds in the room. Give me the coordinates of these two beds.  <b>A:</b> [1.13, 1.64, 0.35, 0.92, 0.03, 1.16], [1.13, 1.64, 0.35, 0.92, 0.03, 1.16]</p>		<p><b>Q:</b> Give me the coordinates of the light brown wooden coffee table.  <b>A:</b> [1.13, 1.64, 0.35, 0.92, 0.03, 1.16]</p>

Figure 6: Qualitative Results.

Fig. 6 presents reconstruction results on the ScanNet dataset, together with three representative 3D vision–language (3D VL) tasks. Specifically, it illustrates (1) 3D Question Answering, where the model answers queries on object counts, locations, and attributes from reconstructed scenes; (2) 3D Dense Captioning, which provides detailed semantic descriptions of rooms and key objects; and (3) 3D Visual Grounding, where the model localizes target objects in 3D space according to textual instructions. These qualitative results demonstrate the model’s capability in scene reconstruction and 3D VL reasoning from video inputs.

### A.2 SUPPLEMENTARY EXPERIMENTS ON RECONSTRUCTION

**Overview.** Since the reconstruction branch not only provides 3D cues for the 3D-MLLM but also explicitly produces point clouds that can serve downstream applications, it is important to assess its individual performance. To evaluate the 3D modeling capability of Vid-LLM, we assess three tasks: camera pose estimation, depth prediction, and point-cloud reconstruction. Depth prediction is crucial to real-scale reconstruction, and together with poses it determines the quality of the recovered point clouds. Following standard protocols, we evaluate poses on Co3Dv2 (Reizenstein et al., 2021)

Table 7: Camera pose evaluation on Co3Dv2 and RealEstate10K.

Method	Co3Dv2			RealEstate10K
	RRA@15↑	RTA@15↑	mAA(30)↑	mAA(30)↑
COLMAP+SG (Sarlin et al., 2020)	36.1	27.3	25.3	45.2
PixSfM (Lindenberger et al., 2021)	33.7	32.9	30.1	49.4
PoseDiff (Lee & Lee, 2024)	80.5	79.8	66.5	48.0
DUST3R (Wang et al., 2024)	94.3	88.4	77.2	61.2
MAS3R (Leroy et al., 2024)	94.6	91.9	81.8	76.4
FLARE (Zhang et al., 2025)	95.4	83.6	78.4	75.3
Fast3R (Yang et al., 2025)	96.2	81.6	75.0	72.7
CUT3R (Wang et al., 2025b)	95.7	84.5	73.3	77.1
Vid-LLM (Ours)	<b>96.8</b>	<b>93.4</b>	<b>88.5</b>	<b>83.1</b>

Table 8: Depth estimation results on the NYU Depth v2 dataset.

Method	$\delta_1 \uparrow$	AbsRel $\downarrow$	RMSE $\downarrow$	$\log_{10} \downarrow$
DPT (Ranftl et al., 2021)	0.904	0.110	0.357	0.045
P3Depth (Patil et al., 2022)	0.898	0.104	0.356	0.043
SwinV2-L (Liu et al., 2022)	0.949	0.083	0.287	0.035
AiT (Ning et al., 2023)	0.954	0.076	0.275	0.033
VPD (Zhao et al., 2023)	0.964	0.069	0.254	0.030
ZoeDepth (Bhat et al., 2023)	0.953	0.075	0.270	0.032
DepthAnything (Yang et al., 2024)	0.984	0.056	0.206	0.024
Vid-LLM(Ours)	<b>0.987</b>	<b>0.025</b>	<b>0.109</b>	<b>0.010</b>

and RealEstate10K (Zhou et al., 2018), depth on the indoor NYU Depth v2 dataset (Silberman et al., 2012), and point-cloud reconstruction on ScanNet (Dai et al., 2017), ensuring consistency with the 3D vision–language benchmarks introduced earlier.

**Baseline.** For 3D reconstruction, we evaluate three subtasks: (i) camera pose estimation, where we compare against geometry-based optimization methods including COLMAP+SG and PixSfM, as well as state-of-the-art learning-based approaches such as PoseDiff, DUST3R, MAS3R, FLARE, Fast3R, and CUT3R; (ii) monocular depth estimation, where we benchmark against DPT, P3Depth, SwinV2-L, AiT, VPD, ZoeDepth, and DepthAnything; and (iii) point-cloud reconstruction, where we consider pose-dependent methods such as MVDNet, GPMVS, Atlas, NeuralRecon, DG-Recon, and PanoRecon, together with pose-free approaches including RCVD, GCVD, COLMAP, Frozen-Recon, and DUST3R, ranging from traditional multi-view geometry to modern learning-based techniques. Notably, both depth and point-cloud evaluations are conducted in real scale.

**Result & Analysis.** Across the three benchmarks, Vid-LLM demonstrates strong reconstruction performance. On camera pose estimation (Tab. 7), it consistently surpasses both traditional optimization pipelines and advanced learning-based models on Co3Dv2 and RealEstate10K, confirming its robustness in preserving reliable multi-view consistency. On monocular depth estimation (Tab. 8), Vid-LLM achieves state-of-the-art results on NYU v2 at real scale, reaching an AbsRel of 0.025, RMSE of 0.109,  $\log_{10}$  of 0.010, and a  $\delta_1$  score of 0.987, representing substantial improvements over prior baselines. On point-cloud reconstruction (Tab. 9), Vid-LLM ranks as the best among pose-free methods on ScanNet, delivering an average improvement of 32% over the second-best approach, and even attains the highest Precision among all methods including pose-dependent pipelines, while maintaining a comparable global F-score. These results collectively indicate that Vid-LLM, despite operating without external poses, produces reliable real-scale depth and point clouds that are both clean and geometrically consistent.

### A.3 IMPLEMENTATION DETAILS

In practice, we adopt DINOv2-L as the visual backbone, consisting of 24 Transformer layers with a hidden dimension of 1024. The projection MLPs use two fully connected layers with an expansion factor of 4 and GELU activation. For implementation, the Global–Frame Attention, camera head, and dense head in the reconstruction branch are adapted from VGGT (Wang et al., 2025a), while the construction of 3D patch representations in the reasoning branch is inspired by the approach used

Table 9: Reconstruction results on the ScanNet dataset.

Method	GT cams	Comp ↓	Acc ↓	Recall ↑	Prec ↑	F-score ↑
MVDNet (Ou et al., 2022)	✓	0.040	0.240	0.831	0.208	0.329
GPMVS (Liu et al., 2023)	✓	<b>0.031</b>	0.879	<b>0.871</b>	0.188	0.304
Atlas (Murez et al., 2020)	✓	0.062	0.128	0.732	0.382	0.499
NeuralRecon (Sun et al., 2021)	✓	0.106	0.073	0.428	0.592	0.494
DG-Recon (Ju et al., 2023)	✓	0.085	<b>0.039</b>	0.476	0.675	0.521
PanoRecon (Wu et al., 2024)	✓	0.089	0.064	0.530	0.656	<b>0.584</b>
RCVD (Kopf et al., 2021)	✗	0.161	0.425	0.164	0.109	0.125
GCVD (Lee et al., 2022)	✗	0.175	0.278	0.178	0.146	0.147
Colmap (Schonberger & Frahm, 2016)	✗	0.142	0.367	0.119	0.267	0.178
FrozenRecon (Xu et al., 2023)	✗	0.092	0.085	0.436	0.336	0.410
DUS3R (Wang et al., 2024)	✗	0.243	0.179	0.284	0.657	0.387
Vid-LLM(Ours)	✗	<b>0.071</b>	<b>0.042</b>	<b>0.634</b>	<b>0.885</b>	<b>0.582</b>

in LLaVA-3D (Zhu et al., 2025). All attention blocks are equipped with FlashAttention to reduce memory usage, and QK-Norm is applied prior to LayerNorm for stability. For data processing, we uniformly sample 32 frames per scene, resize the shorter side to 518, crop the resolution so that both height and width are multiples of 14, and apply standard augmentations including random cropping, color jittering, and horizontal flipping, ensuring augmentation independence across frames. Optimization is performed using AdamW with  $\beta_1 = 0.9$ ,  $\beta_2 = 0.999$ , and weight decay of 0.05, with gradient clipping at 1.0. We further enable mixed-precision training and activation checkpointing to reduce memory consumption.

#### A.4 THE USE OF LARGE LANGUAGE MODELS (LLMs) STATEMENT

Parts of the language in this manuscript were polished with the assistance of Large Language Models (LLMs). The authors have carefully reviewed and verified all LLM-assisted text to ensure accuracy and appropriateness. The intellectual contributions, ideas, and conclusions presented in this work are entirely those of the authors.